Solids Mixing in an Expanded Top Fluid Bed

This study investigated solids mixing of a group A fine powder in a 0.15 m ID expanded top fluid bed with a ferromagnetic tracer. The superficial gas velocity was raised from 0.075 to 1.1 m/s, causing the bed to go through bubbling, slugging, and turbulent fluidization regimes. A countercurrent flow model described the data well at low gas velocities. The bed assumed a more homogeneous appearance at higher gas velocities; a one-dimensional axial dispersion model was used to correlate the data. Axial dispersion coefficients increased with gas velocity. The data agree well with literature data for low gas velocities.

AMOS AVIDAN and JOSEPH YERUSHALMI

Department of Chemical Engineering
The City College of New York
New York, NY 10031

SCOPE

This study investigated the mixing of a typical fluid catalytic cracking (FCC) catalyst, of Geldart's (1973) group A classification, in a 0.15 m ID expanded top fluid bed. The bed operated in the bubbling, slugging, and turbulent fluidization regimes. Most previous studies of solids mixing were limited to the bubbling and slugging regimes. The present work measured solids mixing by using ferromagnetically tagged tracer particles.

Commercial fluid-bed reactors using fine powders often operate in the turbulent fluidization regime when gas velocities exceed 0.3 m/s. This regime is characterized by rapid coalescence of bubbles, good gas-solid contact, and overall homogeneous appearance of the fluid bed. Bubbles are small, especially when a considerable fines fraction (less than 40 μm) is present. The reactor diameter, rather than bubble size, is the dominant scale for describing reactor fluid dynamics.

Solids mixing data are usually correlated by the bubbling and countercurrent flow models. The present study was made to examine how well these models hold at higher gas velocities, when the bed assumes a more homogeneous appearance. The axial dispersion model was also reexamined.

Solids mixing is an important phenomenon because it contributes to the isothermal appearance of gas-solid fluid-bed reactors. Solids and gas mixing are related phenomena. Both play an important role in gas-solid catalytic reactions. In some processes, backmixing of adsorbed products on catalyst particles can adversely affect process selectivity. Solids mixing depends on bed diameter, and this is important in fluid-bed scale-up.

CONCLUSIONS AND SIGNIFICANCE

1. The countercurrent flow model describes solids mixing well in the bubbling fluidization regime. It corresponds to the two-phase appearance of the fluid bed. The phase velocities required by the model can be easily measured by tracer response. Axial solids dispersion coefficient can be calculated from this model. The countercurrent flow model does not require information about bubble size (required by the bubbling bed model). This is advantageous, as bubble size varies with bed geometry and cannot be scaled-up to commercial-size beds.

2. The countercurrent flow model does not describe solids mixing well in the turbulent fluidization regime. Phase velocities are hard to measure. The bed assumes a more homogeneous appearance: bubbles are smaller; they break up and coalesce rapidly. The turbulent appearance of the bed is enhanced for tall beds, and when the solids fines fraction is high (more than 20% less than 40 μm).

3. A one-dimensional Taylor dispersion model fits the data well. The axial dispersion coefficients increase with gas velocity. They agree well with literature data, and with dispersion coefficients obtained from the countercurrent flow model, in the bubbling regime. The data obtained were compared with data from different diameter fluid beds. Axial dispersion coefficients increase with the square root of bed diameter.

4. The ferromagnetic tracer method was applicable to the study of solids mixing of a group A powder. This nondisruptive experimental technique yielded good data in the bubbling, slugging, and turbulent fluidization regimes. The study used a 0.15 m ID expanded top fluid bed. This system is less homogeneous than an external circulation system at gas velocities higher than 1 m/s, when solids entrainment becomes appreciable.

EXPERIMENTAL

Review of Experimental Methods

Solids mixing in a fluid bed can be measured by several experimental techniques (Oki et al., 1977). These techniques are either disruptive or nondisruptive. Disruptive techniques require either the introduction of probes into the fluid bed, or abrupt defluidization of the bed and layer-by-layer analysis (Babu et al., (1973). Defluidization techniques are time-consuming and uncertain; the particles can move significantly during the several seconds required.

Another disruptive technique is isokinetic sampling (van Breugel et al., 1970). It is limited to dilute conveying systems. Other methods include thermistor integrator probes and capacitance probes. The problem with these methods is interference with local flow patterns in the bed. We looked for a nondisruptive technique because of the relatively high gas velocity we planned to investigate.

Correspondence concerning this paper should be addressed to A. A. Avidan who is currently at Mobil Research and Development Corporation, Research Department, Paulsboro, NJ 08066.

Joseph Yerushalmi is currently at PAMA (Energy Resources Development, Ltd.), Tel Aviv 61240, Israel.

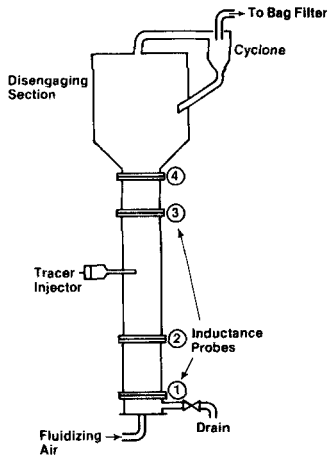

Figure 1. The 152 mm ID expanded top bed.

Some tracer methods have no effect on local flow patterns in the fluid bed if the measurement is external. Photography was used to follow colored particles (Merry and Davidson, 1973), but it yielded information only about the wall region. Radioactive tracers (van Zuillichem et al., 1973; Kondukov et al., 1964) are hazardous materials, and Fitzgerald et al. (1977) claim that they yield noisy data. Strong gamma radiation has to be used (because of the shielding effect of bed material), and adjacent probes pick up distant signals.

Another nondisruptive technique, a ferromagnetic tracer, is described by Razumov et al. (1968). Cranfield (1972) reports the use of a ferromagnetic tracer in a fluid bed of large particles. He observed that the inductance probes used did not initiate flow of particles, or attract particles. We chose a ferromagnetic tracer system, based on a sensitive bridge circuit developed by Fitzgerald, et al. (1977).

Apparatus

We used a 0.15 m ID expanded top fluid bed, made mostly from Plexiglas, Figure 1. This system is similar to some commercial fluid beds. The expanded top causes a reduction in gas velocity, and hence reduces entrainment. The cyclone dipleg in our fluid bed terminated in the expanded top. This system differs from systems with external solids circulation and no expanded tops. The solids in external circulation systems return to the bottom of the fluid bed (e.g., SASOL's Synthol reactor). We observed some differences in solids mixing between the two types of systems (Avidan, 1980). The external circulation system was more homogeneous and more stable than the expanded top system at the higher gas velocities.

The lower part of the bed is a 0.15 m ID column, 3.5 m tall. A cone 0.23 m tall connects the lower part to the expanded top, which is 0.34 m ID and 1.4 m tall. The area increase (by a factor of 5) in the expanded top caused most of the entrained solids to fall back into the fluid bed, even at the highest velocities. Only small amounts of solids were carried to the cyclone. Solids loss was negligible. A fresh batch of solids was loaded into the bed before each run to avoid build-up of the concentration of ferromagnetic tracer. The solids were a typical FCC catalyst, fresh HFZ-20 (Table 1). Before each run, 30 kg of solids were loaded into the bed. Operating bed heights were between 2.7 and 3.5 m.

Air from a 170 kPa blower entered the bed through a carborundum porous plate distributor (eloxate disc, grade 5). The average opening size of the distributor was 50 μm. The pressure drop through the distributor was 2 to 10 kPa, depending on gas velocity. It corresponded to a minimum of 12% of the bed pressure drop. Neither maldistribution nor preferential gas flow was observed above the distributor.

TABLE 1. PROPERTIES OF FRESH HFZ-20 CATALYST

Size Distribution Range (μm)	wt. %
0–20	1.1
20–40	20.1
40–64	47.5
64–80	22.0
80–130	9.0
>130	0.3

Average particle diameter: 49 μm.
Apparent solid density: 1.45 g/cc.
Measured minimum fluidization velocity: 2 mm/s.

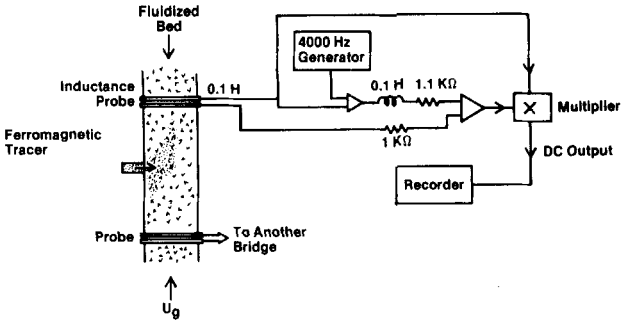

Figure 2. The ferromagnetic tracer system.

The ferromagnetic tracer system is shown in Figure 2. Approximately 0.15 kg of tracer (0.5% of bed inventory) was injected pneumatically into the center of the bed in a short time, typically 0.5 to 1 s. The injection tube was 25 mm ID. Tests were made at three injection air pressures: 380, 240 and 170 kPa. A difference in the tracer response was observed in going from 380 to 240 kPa, but no further change was noted at the lowest pressure. Thus, an injection pressure of 200 kPa was used. The amount of tracer injection air was 1.5–6% of the fluidizing air. No change in the local pressure drop at the time of injection was observed.

Four external probes measured the concentration of ferromagnetic particles, Figure 1. These inductance probes were made from 24-gauge copper wire wrapped around a bed section in nine layers. Probe locations were:

Probe	Distance from Injection, m
1	1.20
2	0.53
3	0.76
4	1.42

Probe 1 was located 0.15 m above the distributor.

The signal from each probe was processed by a bridge element, Figure 2. The bridge used a function multiplier to obtain a linear signal directly proportional to inductance changes. A 4 kHz sine wave excited the bridge whose two legs were a 0.1 H torroid and the 0.1 H inductance probe. Small changes in resistance produced an output 90° out of phase with the excitation voltage, thus producing no net output. An imbalance of the inductance, produced by the passage of ferromagnetic particles near a probe, gave rise to a linear output signal.

The tracer was prepared from finely crushed (−37 μm) manganese-zinc transformer parts. The ferromagnetic powder was incorporated into polyurethane foam to match the bulk density of HFZ-20, then it was crushed and sieved to the same particle size distribution. The resulting tracer powder was free-flowing, much like the catalyst used in the experiments. The tracer was well dispersed in the fluid bed. It did not segregate at any time, even upon defluidization. The force acting on the particles by the probes was negligible.

The probe was sensitive to as little as 5 g of ferromagnetic tracer. The field penetration of the probes insured measurements across the entire bed cross section. The probes tend to give more weight to tracer particles traveling near the wall. This problem is common to most through-the-wall tracer techniques (May, 1959). We assumed that probe reading was proportional to tracer concentration in the cross section. Further details about the experimental setup are given by Avidan (1980).

TABLE 2. RUN CONDITIONS

Run No.	Superficial Gas Velocity (m/s)	Average Bed Voidage	Fluidization Regime
E1	0.075	0.51	Bubbling
E2	0.24	0.56	Bubbling/slugging
E3	0.48	0.61	Slugging
E4	0.48	0.61	Slugging
E5	0.84	0.66	Slugging/turbulent
E6	0.86	0.67	Slugging/turbulent
E7	0.86	0.66	Slugging/turbulent
E8	1.10	0.70	Turbulent

TABLE 3. EXPERIMENTAL RESULTS

	Time(s) for tracer concentration to reach value															
	Probe				Probe				Probe				Probe			
$c(t)/C_\infty$	1	2	3	4	1	2	3	4	1	2	3	4	1	2	3	4
	Run E1				Run E2				Run E3				Run E4			
0.1	5.0	2.0	0.5	2.4	3.6	1.2	0.5	1.3	2.0	0.1	0.3	0.9	3.0	0.8	0.4	1.0
0.5	7.0	2.1	1.2	3.2	3.7	1.4	0.6	2.2	3.6	0.2	0.9	1.9	4.0	1.0	0.5	1.8
0.9	7.4	2.2	1.3	5.7	3.8	1.6	1.4	7.0	5.8	0.5	1.0	6.0	8	1.2	0.6	5.0
Max. at (s)	8.1	3.2	3.5	8.7	4.3	1.8	2.6	10	10	3.0	3.0	11	11	1.5	2.0	8.0
$c(t)/C_\infty$ at max.	2.9	3.0	2.1	1.33	2.1	2.7	1.2	1.0	1.0	2.0	1.3	1.0	1.0	1.1	1.6	1.0
	Run E5				Run E6				Run E7				Run E8			
0.1	1.6	0.7	0.3	0.8	2.2	0.6	0.3	0.8	2.0	0.9	0.4	1.0	1.4	0.3	0.4	0.9
0.5	2.5	0.9	0.5	1.6	2.8	1.0	0.4	1.5	3.0	1.0	0.6	2.2	1.8	0.5	0.6	2.8
0.9	4.1	1.0	0.6	4.5	4.8	1.1	0.5	7.0	4.0	1.4	0.8	6.0	4.0	0.6	1.2	5.0
Max. at (s)	5.0	2.0	1.2	6.0	5.4	1.2	0.8	10	5.2	2.5	1.1	8.4	4.5	1.0	1.5	12
$c(t)/C_\infty$ at max	1.0	1.4	1.5	1.0	1.0	1.1	1.7	1.0	1.0	1.2	1.5	1.0	1.0	1.3	1.3	1.0

RESULTS

Run conditions are listed in Table 2. The transition from one fluidization regime to the next was gradual. It also depended on axial position. For example, in run E2 the lower part of the bed was in the bubbling regime, while the top was slugging. The transition to turbulent fluidization was observed at approximately 0.85 m/s. This is also the velocity at which the slope of the bed expansion curve changed from 10 to 5. We defined such a change as regime transition using a modified Richardson-Zaki approach (Avidan and Yerushalmi, 1982).

Two strip chart recorders (two channels each) simultaneously recorded the data. The results are tabulated in Table 3. Strip chart recordings of three of the runs are shown in Figures 3–5. The time scale is shown on the righthand side of the chart. The lefthand event marker shows when the tracer injection air solenoid was open. Time zero is defined as the mean of this injection interval.

Figure 3 shows the results for a bubbling bed. Channel 2 shows one large peak after approximately 3 seconds. The same peak is recorded 5 seconds later by channel 1. Both downstream channels show a different behavior. While the tracer response is still underdamped, it is more spread out. Moreover, periodic dips in the tracer concentration suggest the passage of bubbles. These dips were not observed in the lower channels. Bubbles coalesce and grow larger as they pass through the bed.

Figure 4 shows the bed at a gas velocity of 0.24 m/s. The mechanism of bubble growth is still evident: the bed is slugging in the vicinity of probe 4. Figure 5 shows the bed undergoing transition from slugging to turbulent fluidization. The frequency of fluctuations seems to be the same throughout the bed at higher gas velocities. Except for some occasional big bubbles, this frequency is no longer associated with individual bubbles or slugs. It confirms the visual observation that the transition to turbulence is associated with a more random, homogeneous appearance of the bed. Bubbles are smaller overall than the slugs observed previously. They assume twisted shapes and undergo rapid breakup and coalescence.

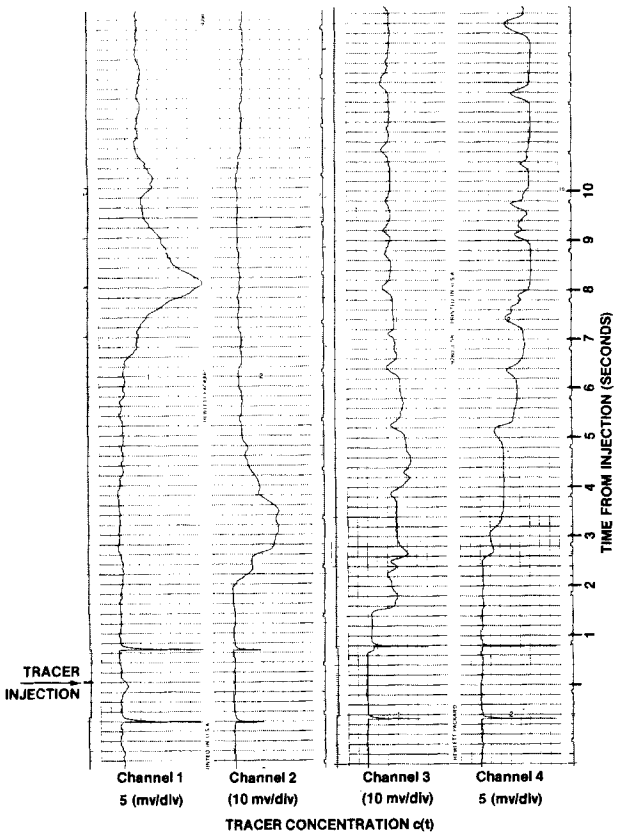

Figure 3. Tracer response in the bubbling regime; run E1.

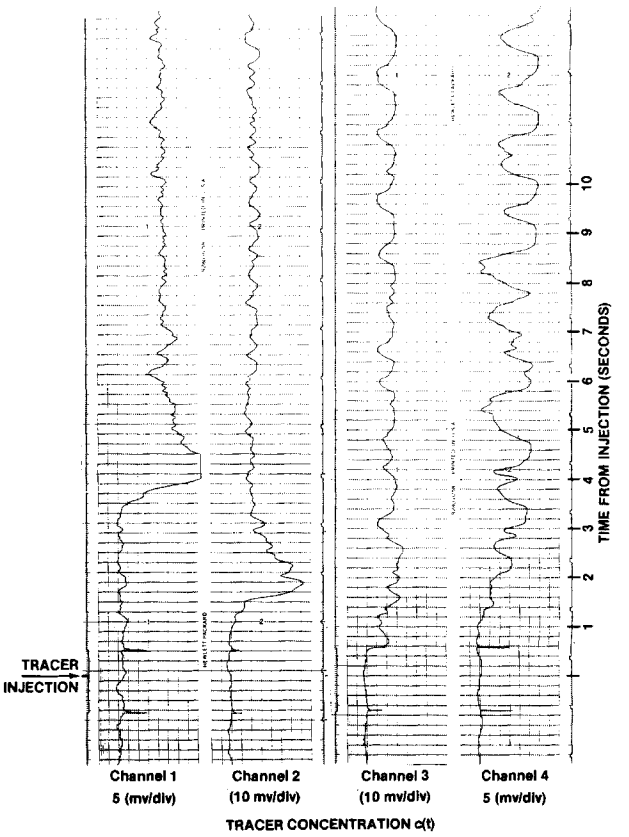

Figure 4. Tracer response in the bubbling/slugging regime; run E2.

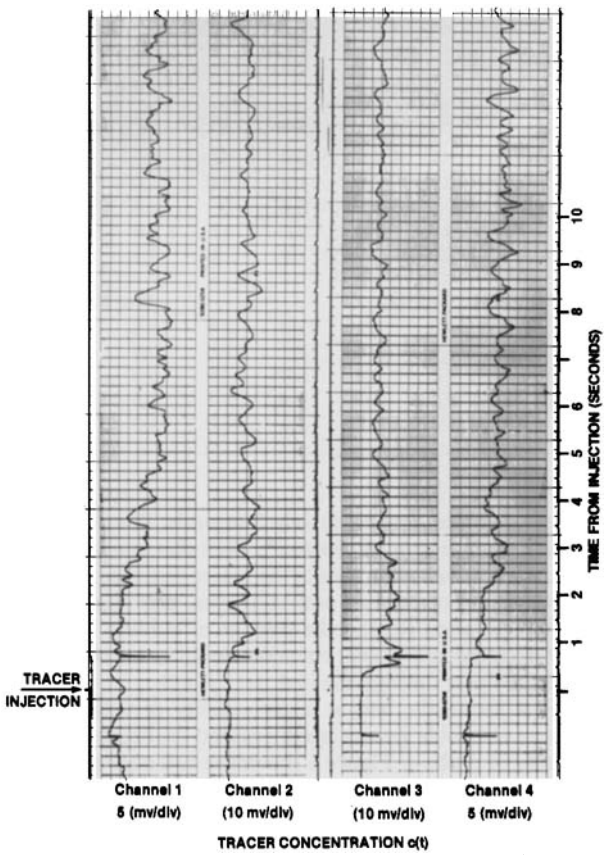

Figure 5. Tracer response in the turbulent regime; run E6.

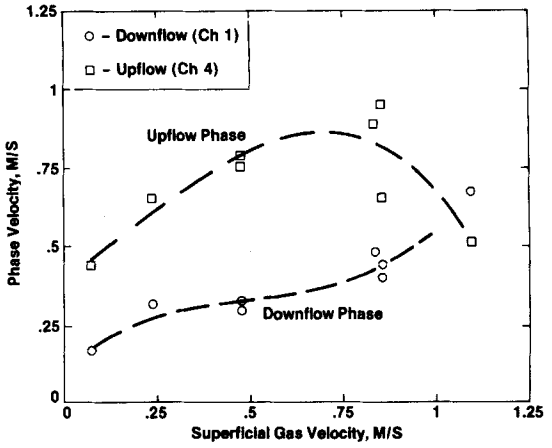

Figure 6. Phase velocities.

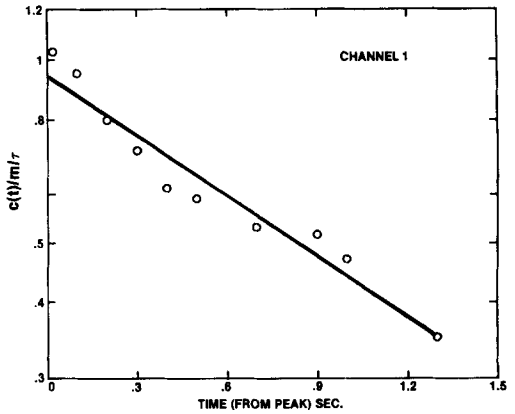

Figure 7. Tracer response by the two-phase method; channel 1, run E1.

SOLIDS MIXING MODELS

Potter (1971) describes various models used to correlate solids mixing. Early attempts included simple one parameter models; e.g., tanks in series or dispersion models. These could not account for the heterogeneous nature of the fluid bed. A dispersion model cannot describe considerable gas bypassing. It cannot predict conversions lower than that of a completely mixed tank reactor. And such gas bypassing was observed in shallow fluid beds, in beds of coarse particles, or in beds poor in fines (e.g., many FCC regenerators).

"Bubbling" models (Kunii and Levenspiel, 1969) include several parameters which depend on the properties of bubbles. It is not easy to predict bubble size in large fluid beds, especially in commercial units. The more homogenous appearance of the turbulent fluidization regime makes this task even harder.

The Counter-Current Flow Model

The counter-current flow model was introduced by van Deemter (1967). Solids are in two distinct phases: upflowing and downflowing. A mass balance for the system is shown in the appendix. We solved van Deemter's equations by the method of characteristics to obtain the solution for a tracer pulse response. The solution moves with the velocity of the phase, Eq. A11.

Solids velocity of the downflow phase can be easily obtained from the data at the two lowest gas velocities, Figures 3 and 4. At higher gas velocities, the shape of the upstream channels response curves looks more like the downstream ones: more spread out, and eventually overdamped, Figure 5. Thus, it is not clear what the phase velocities are at gas velocities higher than 0.5 m/s. We arbitrarily chose the phase velocity to represent the time when the response was 50% of the final value $[c(t)/c_\infty = 0.5]$.

These phase velocities are plotted vs. the superficial gas velocity in Figure 6. The velocity of the upflow phase is larger than the superficial gas velocity in the bubbling regime. And it seems to peak in the turbulent regime. The velocity of the downflow phase is approximately one-half the superficial gas velocity. The phase velocities are equal at a superficial gas velocity of 1.1 m/s.

The difficulty in obtaining clearly defined phase velocities prevents us from analyzing all of our results by the counter-current flow model. We tried it for the two lowest gas velocities. Equation A11 can be rewritten as:

$$\log \frac{c(t)}{m/\tau} = -t/\tau \tag{1}$$

The decline in tracer response (from the maximum) for one upstream channel is plotted on a semilog scale in Figure 7. The slope of the curve yields τ, and the effective dispersion coefficient is calculated from:

$$D_{SP} = \tau f v^2 \tag{2}$$

The results for runs 1 and 2 are listed in Table 4. The dispersion coefficients are equal to the values obtained later by the turbulent dispersion model at the lowest gas velocity. We could not apply the counter-current flow model at higher gas velocities because of the uncertainty in the phase velocities. The shape of the response curve at the higher gas velocities (especially when overdamped) makes it difficult to analyze by this model.

TABLE 4. DISPERSION COEFFICIENTS FROM COUNTER-CURRENT FLOW MODEL

Run	Channel	τ (s)	D_{sp} (m²/s)
E1	1	2.04	0.06
	2	2.09	0.06
E2	1	3.33	0.20
	2	2.00	0.12

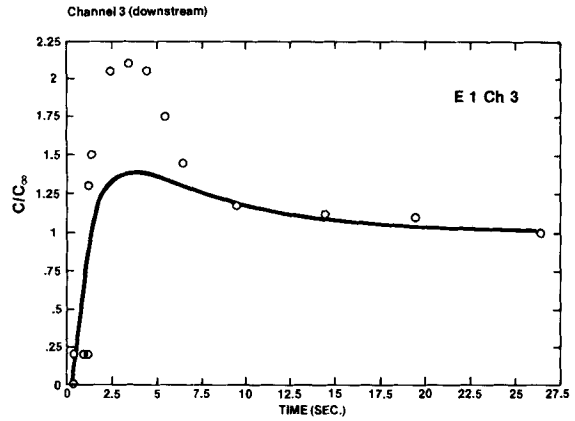

Figure 8a. The dispersion model; channel 3 (downstream), run E1.

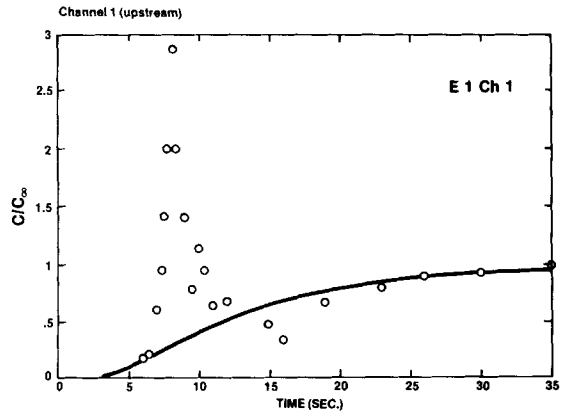

Figure 8b. The dispersion model; channel 1 (upstream), run E1.

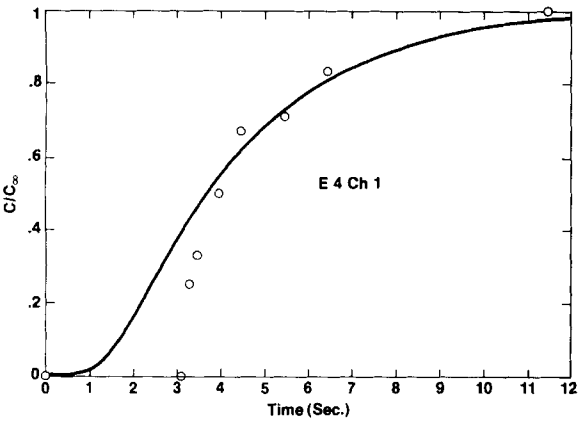

Figure 9a. The dispersion model; channel 1, run E4.

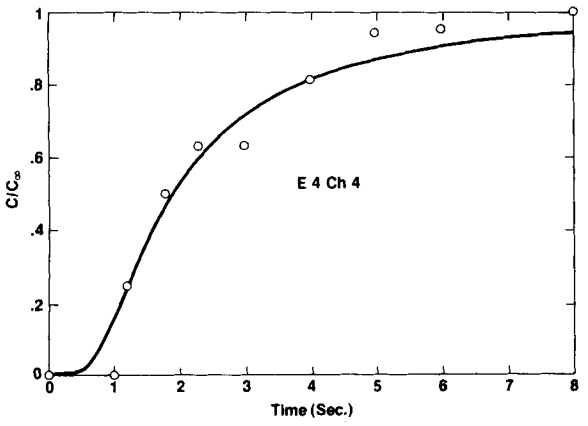

Figure 9b. The dispersion model; channel 4, run E4.

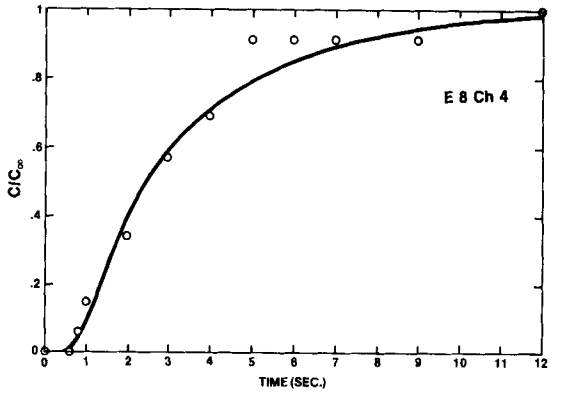

Figure 10a. The dispersion model; channel 4 (downstream), run E8.

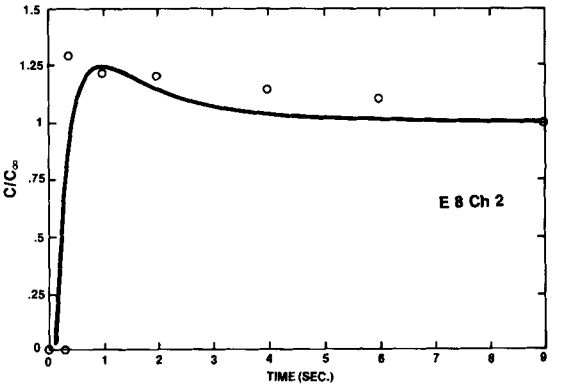

Figure 10b. The dispersioin model; channel 2 (upstream), run E8.

The Turbulent Dispersion Model

The more homogeneous appearance of the bed at the higher gas velocities led us to reexamine the dispersion model. The rapid breakup of bubbles ensures that no gross gas bypassing will occur in the turbulent fluid bed, if it is tall enough. This is especially true when the solids fines fraction is high (over 20% less than 40 μm). Our experiments with a gas tracer (Cankurt and Yerushalmi, 1978) show that the length of a "mixing cell," or turbulent eddy length, decreases rapidly as the gas velocity is raised. The fluid bed appears homogeneous if bed height is much larger than this mixing cell. In the turbulent fluidization regime this length is of the same order of magnitude as the bed diameter. We operated at bed height-to-diameter ratios of 18-23.

The dispersion mechanism can be described as one-dimensional Taylor dispersion:

$$D_{SP}\frac{\partial^2 C}{\partial X^2}=\frac{\partial C}{\partial t} \tag{3}$$

D_{SP} is the effective solids dispersion coefficient. The solution for a pulse injection of tracer is (May, 1959):

$$\frac{C}{C\infty}=1+2\sum_{n=1}^{\infty}\exp\left(-n^2\pi^2\frac{D_{SP}t}{L^2}\right)\cos\frac{n\pi}{L}x \tag{4}$$

We calculated D_{SP} by matching the measured response curves to the theoretical solution. A comparison of the data with the dispersion model in the bubbling regime is shown in Figure 8. The dispersion model fits the data

TABLE 5. EFFECTIVE AXIAL DISPERSION COEFFICIENT D_{sp} (m²/s)

Run	Channel 1	2	3	4	Average D_{sp}
E1	N.A.	0.06	0.075	0.09	0.075
E2	0.075	N.A.	0.09	0.093	0.086
E3	0.084	0.084	0.084	0.084	0.084
E4	0.075	0.075	0.13	0.093	0.093
E5	0.13	N.A.	0.16	0.16	0.150
E6	0.14	N.A.	N.A.	0.16	0.150
E7	0.12	N.A.	0.16	0.14	0.140
E8	0.14	0.14	0.17	0.15	0.150

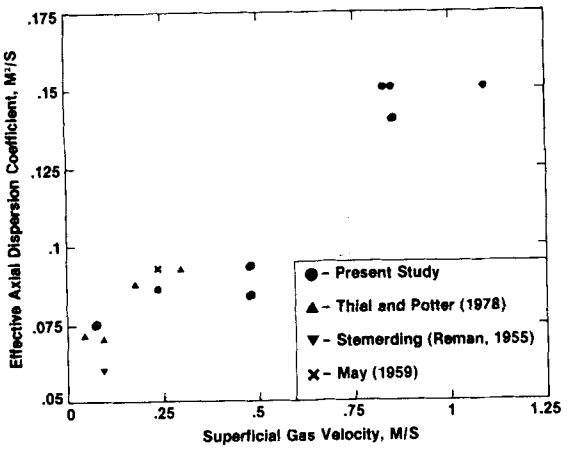

Figure 11. Dispersion coefficients vs. gas velocity.

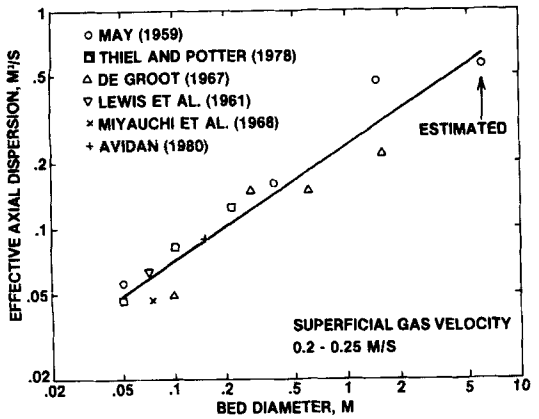

Figure 12. Effect of bed diameter on solids dispersion coefficients.

poorly at this gas velocity; the discrepancy suggests that the flow is segregated. The counter-current flow model represents the flow better in this regime.

The dispersion model fits the data well at higher gas velocities, Figures 9 and 10. This corresponds to our observation of the change in behavior of the fluid bed, from a two-phase representation in the bubbling fluidization regime to a homogeneous representation at the higher gas velocities.

The calculated dispersion coefficients are listed in Table 5. The agreement among the dispersion coefficients calculated at the four probes is good. The two farther probes (channels 1 and 4) gave somewhat better results, as expected. The top dispersion coefficients (channels 3 and 4) seem somewhat larger than the bottom ones. We used the average to represent the effective axial dispersion coefficient at each gas velocity.

We compared our results with data from similar diameter beds in Figure 11. The agreement between our data and the data of Thiel and Potter (1978), Stemerding (Reman, 1955), and May (1959) is good. The dispersion coefficient increases with gas velocity. (We interpolated the data of Thiel and Potter between two bed diameters used by them: 0.102 m and 0.218 m.)

The effect of bed diameter on the axial dispersion coefficient is large. Data at one gas velocity (0.2–0.25 m/s) are shown in Figure 12. The axial dispersion coefficient increases with the square root of bed diameter.

ACKNOWLEDGMENT

This work was supported by the U.S. Department of Energy under contract EX-76-S-01-2340. T. Fitzgerald provided the inductance bridge used.

APPENDIX

The Countercurrent Flow Model

A mass balance for the counter-current flow model yields (van Deemter, 1967):

$$f\frac{\partial c}{\partial t} + fv\frac{\partial c}{\partial x} + k(c - C) = 0 \tag{A1}$$

$$F\frac{\partial C}{\partial t} + FV\frac{\partial C}{\partial x} + k(C - c) = 0 \tag{A2}$$

The interchange coefficient between the two phases is k. For large values of t, and if little carryover from the fluid bed is experienced, the effective dispersion coefficient is:

$$D_{SP} = \frac{(fv)^2}{k(f + F)} = \frac{(FV)^2}{k(f + F)} \tag{A3}$$

Note that the phase velocities, the volume fractions, and the interchange coefficient are needed to calculate the dispersion coefficient. Equations A1 and A2 were solved by the method of characteristics (Avidan, 1980) with the following additional equations:

$$dc = \frac{\partial c}{\partial x}dx + \frac{\partial c}{\partial t}dt \tag{A4}$$

$$dC = \frac{\partial C}{\partial x}dx + \frac{\partial C}{\partial t}dt \tag{A5}$$

To obtain the chracteristic lines the determinant of these four equations was set equal to zero, yielding:

$$Vv + \left(\frac{dx}{dt}\right)^2 - (v + V)\frac{dx}{dt} = 0 \tag{A6}$$

or the solution moves with the velocity of the phase:

$$\frac{dx}{dt} = V \qquad \frac{dx}{dt} = v \tag{A7}$$

To get the solution along the characteristic line, the numerator is set equal to zero, yielding:

$$k(V - f)c + f(V - v)\frac{dc}{dt} = k(V - v) \tag{A8}$$

The Laplace transform of Eq. A8 yields:

$$\frac{c(s)}{C(s)} = \frac{1/\tau}{1/\tau + s} \tag{A9}$$

where s is the transformed time and

$$\tau = \frac{f}{k} \tag{A10}$$

For a pulse injection of a quantity of tracer, m, in one phase (say the upflow phase) the tracer concentration in the other phase is:

$$c(t) = \frac{m}{\tau}e^{-t/\tau} \tag{A11}$$

This solution moves with the velocity of the phase.

NOTATION

c = tracer volume fraction, downflow phase
C = tracer volume fraction, upflow phase
$c(t)$ = tracer concentration near a probe, mV
c_∞ = tracer concentration at steady state, mV
D_{SP} = effective axial solids dispersion coefficient, based on solids phase area
f = solids volume fraction, downflow phase
F = solids volume fraction, upflow phase
k = interchange coefficient
L = bed height
m = volume fraction of injected tracer
n = index in Eq. 4
t = time
v = downflow phase velocity
V = upflow phase velocity
x = axial coordinate

Greek Letters

ϵ = void fraction
τ = characteristic time, Eq. A10

LITERATURE CITED

Avidan, A. A., "Bed Expansion and Solids Mixing in High Velocity Fluidized Beds," Ph.D. Dissertation, The City College of New York (1980).

Avidan, A. A., and J. Yerushalmi, "Bed Expansion in High Velocity Fluidization," *Powder Tech.*, **32**, 223 (1982).

Babu, S. P., et al., "Solids Mixing in Batch Operated Tapered and Non-Tapered Gas Fluidized Beds," *AIChE Symp. Ser. 128*, **69**, 49 (1973).

Cancurt, N. T., and J. Yerushalmi, "Gas Backmixing in High Velocity Fluidized Beds," *Fluidization* (Proc. 2nd Eng. Found. Conf.), J. F. Davidson and D. L. Keairns, eds., Cambridge Univ. Press (1978).

Cranfield, R. R., "A Probe for Bubble Detection and Measurement in Large Particle Fluidized Beds," *Chem. Eng. Sci.*, **27**, 239 (1972).

de Groot, J. H., "Scaling Up of Fluidized Bed Reactors," *Proc. Int. Symp. Fluidization*, A. A. H. Drinkenburg, ed., 348, Netherlands Univ. Press, Eindhoven (1967).

Fitzgerald, T., N. Catipovic, and G. Jovanovic, "Fluidized Bed Test Facility—Report on Instrumentation," supported by EPRI, Oregon State Univ., Corvalis, OR (1977).

Geldart, D., "Types of Gas Fluidization," *Powder Tech.*, **7**, 285 (1973).

Kondukov, N. B., et al., "An Investigation of the Parameters of Moving Particles in a Fluidized Bed by a Radioisotopic Method," *Int. Chem. Eng.*, **4**(1), 43 (1964).

Kunii, D., and O. Levenspiel, *Fluidization Engineering*, John Wiley Sons, New York (1969).

Lewis, W. K., E. R. Gilliland, and H. Girouard, "Heat Transfer and Solids Mixing in a Bed of Fluidized Solids," *Chem. Eng. Progr. Symp. Ser. 38*, **58**, 87 (1961–62).

May, W. G., "Fluidized-Bed Reactor Studies," *Chem. Eng. Progr.*, **55**(12), 49 (1959).

Merry, J. M. D., and J. F. Davidson, "Gulf Stream Circulation in Shallow Fluidized Beds," *Trans. Inst. Chem. Engrs.*, **51** (1973).

Miyauchi, T., H. Kaji, and K. Saito, "Fluid and Particle Dispersion in Fluid-Bed Reactors," *J. Chem. Eng.* (Japan), **1**(1), 72 (1968).

Oki, K., W. P. Walawender, and L. T. Fan, "The Measurement of Local Velocity of Solid Particles," *Powder Tech.*, **18**, 171 (1977).

Potter, O. E., "Mixing," *Fluidization*, J. F. Davidson and D. Harrison, eds., Academic Press, London (1971).

Reman, G. H., "Effect of Gas and Solid Mixing in Fluidized Beds on Chemical Reactions," *Chem. and Ind.*, 46 (Jan. 15, 1955).

Razumov, I. M., et al., "The Flow Structures in Reactors with Concurrent Gas and Solids Flow," *Khim. Prom.* **6**, 405 (1968).

Thiel, W. J., and O. E. Potter, "The Mixing of Solids in Slugging Gas Fluidized Beds," *AIChE J.*, **24**(4), 561 (1978).

van Breugel, J. W., J. J. M. Stein, and R. J. de Vries, "Isokinetic Sampling in a Dense Gas-Solids Stream," *Proc. Inst. Mech. Engrs.*, **184**, part 3C, 18 (1969–1970).

van Deemter, J. J., "The Counter-Current Flow Model of a Gas-Solids Fluidized Bed," *Proc. Int. Symp. on Fluidization*, A. A. H. Drinkenburg, ed., Netherlands Univ. Press, Eindhoven (1967).

van Zuillichem, D. J., G. H. Bleumink, and J. G. de Sewart, "Slip Velocity Measurements by a Radiotracer Technique in Vertical Conveying Systems," Pneumotransport 2, BHRA Fluid Engineering Conf., Bedford, England (1973).

Manuscript received Apr. 14, 1982; revision received June 3, 1984, and accepted June 3.